AIAA Propulsion and Energy Forum
August 9-11, 2021, VIRTUAL EVENT
AIAA Propulsion and Energy 2021 Forum

10.2514/6.2021-3285

Modeling and Simulation of Novel Electric/Hybrid Electric Multicopter Architectures for Urban Air Mobility

Etienne Demers Bouchard[1] and Johannes Verberne[2]
Aerospace Systems Design Laboratory, Georgia Tech, Atlanta Georgia USA

Matilde D'Arpino[3]
The Ohio State University Center for Automotive Research, Columbus, Ohio USA

Metin Ozcan[2]
Aerospace Systems Design Laboratory, Georgia Tech, Atlanta Georgia USA

Francesco Porpora[4]
University of Cassino and Southern Lazio, Cassino, FR, Italy

Jonathan Gladin[5] and Srujal Patel[5]
Cedric Justin[5] and Dimitri Mavris[6]
Aerospace Systems Design Laboratory, Georgia Tech, Atlanta Georgia USA

This paper introduces a dynamic simulation environment developed for novel multi-copter aircraft architectures. The development is motivated by the need to better understand the safety implications of architectural design choices and to provide a formal reliability assessment framework for new Vertical Take-Off and Landing (VTOL) concepts able to consider various airframe and subsystems dynamic behavior. The concepts of interests are different multi-copters configurations investigated by NASA and featuring either electric, hybrid electric, or turboshaft driven powertrains. The simulation environment is a time-marching dynamic simulator formulated using physics-based subsystem models for the batteries, electric motors, turboshaft engines and electric generators. Identified fault modes are integrated into the subsystem models for subsequent use during reliability assessments. The impacts of subsystem faults are propagated to the vehicle flight dynamic response for analysis of their impact on the ability of the vehicle to sustain safe operations. Detailed features of the electric quadrotor model are provided to illustrate the simulation capabilities. Some faults are inserted on the different aircraft in hover and the subsystems behavior is successfully propagated at the vehicle level.

[1] Postdoctoral Researcher, School of Aerospace Engineering, Georgia Institute of Technology
[2] Graduate Research Assistant, School of Aerospace Engineering, Georgia Institute of Technology
[3] Research Scientist, Ohio State University, Center for Automotive Research
[4] PhD candidate, University of Cassino and Southern Lazino, Cassino FR, Italy
[5] Research Engineer II, School of Aerospace Engineering, Georgia Institute of Technology, AIAA Member
[6] S.P. Langley Distinguished Regents Professor and Director, ASDL, School of Aerospace Engineering, Georgia Institute of Technology, and AIAA Fellow

Nomenclature

BMS	=	Battery Management System
BP	=	Battery Pack
DET	=	Dynamic Event Tree
ED	=	Electric Drive
EM	=	Electric Motor
EMF	=	ElectroMotive Force
ESC	=	Electronic Speed Controller
FMECA	=	Failure Mode, Effects & Criticality Analysis
FOC	=	Field Oriented Control
FOD	=	Foreign Object Damage
FTA	=	Fault Tree Analysis
HOGE	=	Hover Out of Ground Effect
IRP	=	Intermediate Rated Power
LQI	=	Linear Quadratic Integral
LQR	=	Linear Quadratic Regulator
MCP	=	Maximum Continuous Power
MRP	=	Maximum Rated Power
NASA	=	National Aeronautics and Space Administration
NDARC	=	NASA Design and Analysis of Rotorcraft
NPSS	=	Numerical Propulsion System Simulation
PI	=	Proportional-Integral
PMSM	=	Permanent Magnet Synchronous Motor
ROC	=	Rate of Climb
RPM	=	Revolutions Per Minute
RVTL	=	Revolutionary Vertical Lift Technology
SIMPLI-FLYD	=	SIMPLIfied FLight dYnamics for conceptual Design
SLS	=	Sea Level Static
u	=	Control input
UAM	=	Urban Air Mobility
V	=	Velocity
VTOL	=	Vertical Take-Off and Landing
WATE	=	Weight Analysis of Turbine Engines
x	=	States
β	=	Rotor flapping angle
τ	=	Torque
Ω	=	Rotor angular velocity

I. Introduction

Urban Air Mobility (UAM) services are defined as the transportation of passengers or cargo aboard low-capacity vehicles over short distances, typically within metropolitan areas and their immediate surroundings. The objective of these UAM services is to bypass and possibly alleviate ground traffic congestion and provide fast, frequent, efficient, and affordable transportation to commuters. The recent convergence of new technologies ranging from energy storage to autonomy, and from flight controls to more sustainable electric and hybrid-electric powertrains brings these new services within reach. The aerospace industry has widely embraced this new breed of operations and more than three hundred aircraft designs are currently at various stages of development, certification, or testing.

Most of the proposed vehicles feature a Vertical Take-Off and Landing (VTOL) capability to enable operations within densely populated environments where the ground footprint of the supporting ground infrastructure can be severely constrained. However, the vehicle and powertrain configurations vary significantly amongst the proposed vehicles. Because these vehicles will be operated close to the ground and in close proximity to people over densely populated cities, research entities such as NASA are interested in understanding the safety benefits of each of these

vehicle configurations. To aid in this research and to provide common baselines for the industry, the National Aeronautics and Space Administration (NASA) developed four concept vehicles [1] as part of the Revolutionary Vertical Lift Technology (RVLT) project to identify crucial technologies, define research requirements, and explore a range of propulsion systems. Recently, Boeing examined various faults and failures associated with the powertrains of these four proposed RVLT concepts [2]. Following this previous research, a number of safety and reliability questions associated with broader powertrain configuration differences remain. To address the safety implications of these configuration differences, the present research proposes to explore the safety and reliability impact of three major vehicle configuration options: the number of rotors, the selection of rotor thrust control, and the propulsion architecture.

The technical approach is divided into two phases: a system modeling phase and a safety assessment process phase [3, 4]. The system modeling focuses on defining the details of the propulsion and flight control systems for three configurations of interest. The objective of the system modeling process is the generation of vehicle dynamic models that can then be used to simulate a variety of components failures and system failures and their effect on the vehicle. The modeling of the various vehicle systems also provides inputs to the safety assessment through dynamic vehicle response evaluation after fault occurrence, which focuses on the identification of hazards and failure modes, the probability of occurrence of these failures, and their potential impacts. The outcome of these failures is categorized into the traditional minor, major, critical, and catastrophic nomenclature. Mitigation actions taken by flight crews following failures, such as diversion to nearby alternate vertiports, are accounted for when quantifying the risk of subsequent failures having potentially catastrophic outcomes. The present paper details the first phase which is the system modeling process to create a dynamic model of several quadrotor configurations and associated subsystems. There reader is referred to [3] and [4] for more details about the safety assessment process.

II. Background and Motivation

A. Mission

Urban Air Mobility missions consists of high tempo operations featuring short hops within a metropolitan area. As a result, the flights are typically short and the mission profile retained for analysis is depicted in Figure 1. The mission consists of a vertical takeoff, a climb at a climb rate 900 ft/min, a cruise and a descent and landing at the destination. The climb and cruise speeds are specific to each vehicle, with the cruise speeds set at the vehicle's best range speed. This leg repeats twice to simulate an outbound flight followed by an inbound flight. A final reserve is added at the end of the mission and is used for sizing purposes. Timed hovers are performed at locations 2, 5, 6 taking 10, 40 and 15 seconds respectively. These hover conditions are repeated for the second leg of the mission as well.

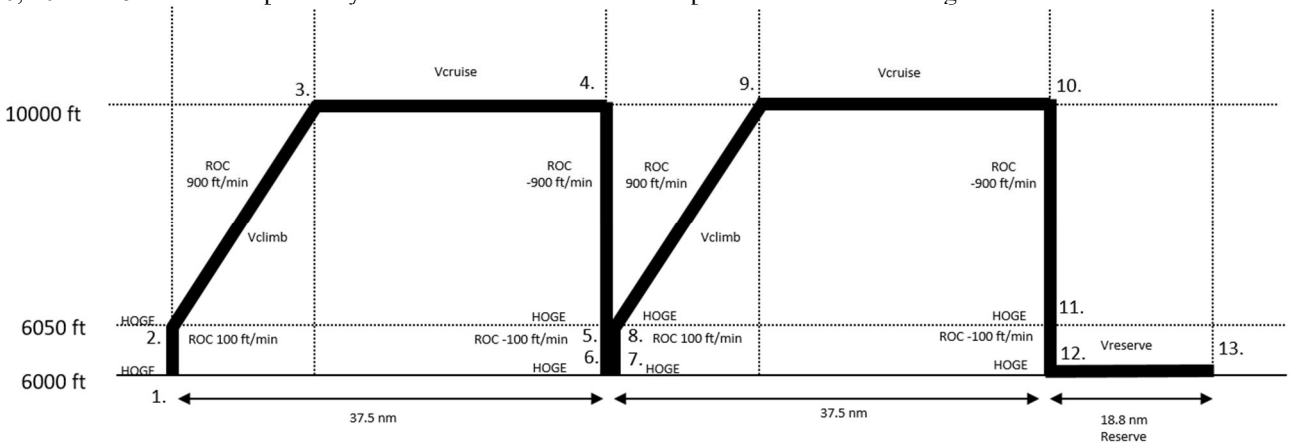

Figure 1 UAM mission profile

B. Definition of the vehicle architectures

The electrification of rotorcraft concepts opens up new architectural alternatives for VTOL missions. Six vehicles capable of the mission were identified as concepts of interest for the reliability analysis: three variable pitch quadrotors with different powertrain configurations, a variable pitch and a variable RPM hexacopters, and finally a variable RPM octocopter. This paper focuses on the three quadrotor concepts and includes an all-electric quadrotor concept, a series-hybrid turbogenerator-battery concept, and a turboshaft driven concept. All three configurations feature collective

pitch control for he rotor as well as a mechanical link between rotors, referred to as cross-shafting. General configuration details and information on power and gross weight are provided in Table 1 and Table 2, respectively.

Table 1: Quadcopter vehicles as provided by NDARC

Aircraft	Number of rotors	Control Strategy	Power source	Motors and Transmission
Electric quadrotor	4	Collective pitch	Battery	Four electric motors, mechanically linked (cross shafting)
Series-hybrid quadrotor	4	Collective pitch	Turbogenerator and a battery	Four electric motors, mechanically linked (cross shafting)
Turboshaft-driven quadrotor	4	Collective pitch	Two turboshaft engines	Rotors driven by two turboshafts, mechanically linked (cross shafting)

Table 2: Quadcopter power and gross weight per configuration as provided by NDARC

Configuration	Engine/Motor Power	Gross Vehicle Weight
Electric quadrotor	112 hp (4x)	6,469 lb
Series-hybrid quadrotor	107 hp (4x)	5,115 lb
Turboshaft-driven quadrotor	240 hp (2x)	3,734 lb

A conceptual sizing of each of these vehicles was performed by NASA through the NASA Design and Analysis of Rotorcraft (NDARC) software [5]. A rendering of the quadrotor vehicles can be seen in Figure 2.

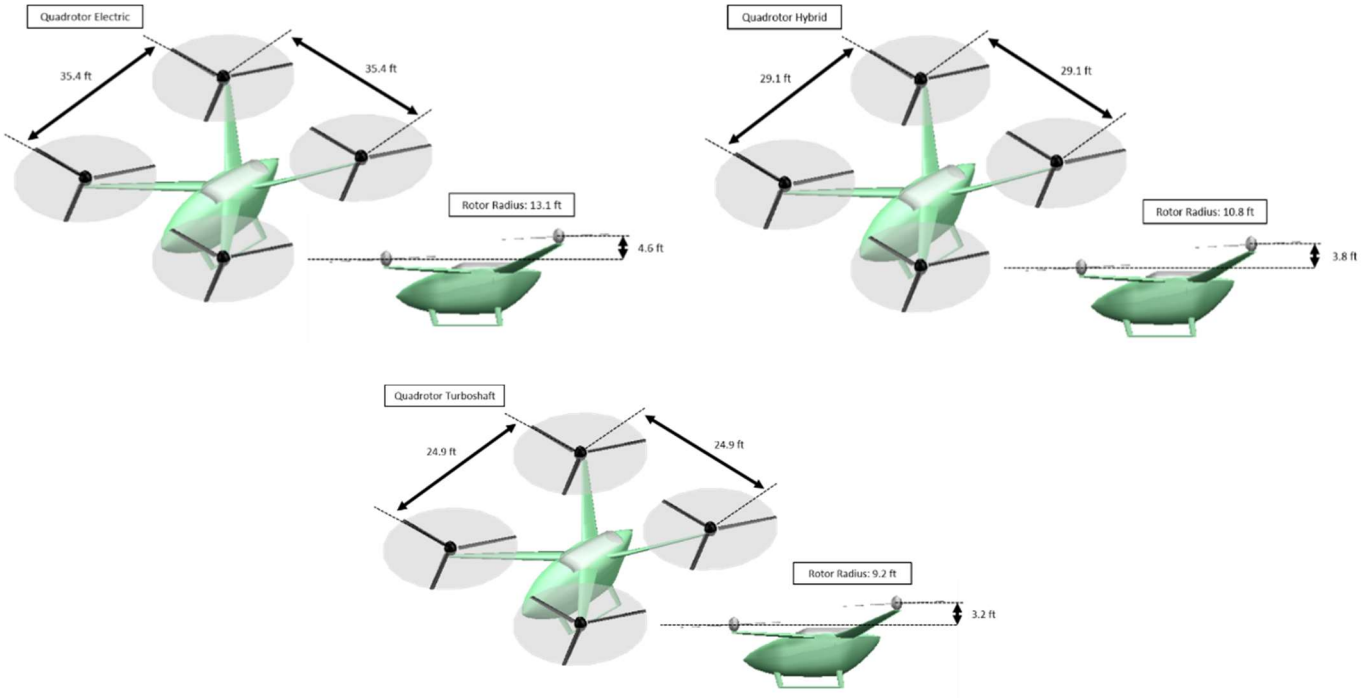

Figure 2 Aircraft overview: electric (top left), series-hybrid (top right) and turboshaft-driven (bottom) quadrotors

III. Dynamic Modeling for UAM Vehicles

A. Simulation Environment Overview

A dynamic simulation environment was developed to virtually fly missions and inject component failures to analyze how the vehicle reacts to the faults. The architecture of the dynamic simulation environment is provided in Figure 3 Schematic representation of the dynamic simulation environment. The environment includes an atmospheric wind and wind-gust model, a guidance and navigation module, a vehicle controller, and an aircraft dynamics module. The aircraft dynamics module is made of an airframe dynamics model and a transmission model. Depending on the vehicle propulsion system, the aircraft dynamics module can also include an electric drive model, a turboshaft model, or a battery model. The following subsections provide more detail on the simulation environment.

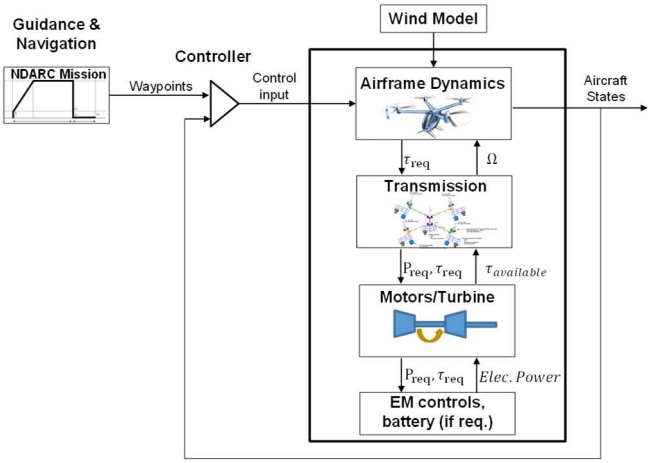

Figure 3 Schematic representation of the dynamic simulation environment

B. Vehicle Modeling

A crucial component for the reliability analysis is the dynamic vehicle model. The dynamic model of the vehicle is a subsystem based and physics-driven time marching simulator. The main model components are the airframe, the controller and navigation modules, and the powertrain. The powertrain can be electric, series-hybrid or turboshaft based.

1. Airframe Dynamics

The starting point for the vehicle model is the airframe dynamic model. The model is based on the SIMPLI-FLYD ('SIMPLIfied FLight dYnamics for conceptual Design') dynamic models provided by NASA [6]. A schematic representation of the dynamic model is illustrated in Figure 4. The dynamic response of the aircraft is provided as a function of the current states, control input, torque input at the rotor and wind condition. The aircraft states consist of the rotor flapping angles, aircraft translational velocities, aircraft rotational velocities and positions, and the angular velocities of the rotors. The control input follows conventional helicopter control using collective, cyclic longitudinal, cyclic lateral and pedal input at the rotor level. The dynamic model is provided as piecewise with advancing velocity linear coefficient about the trimmed conditions.

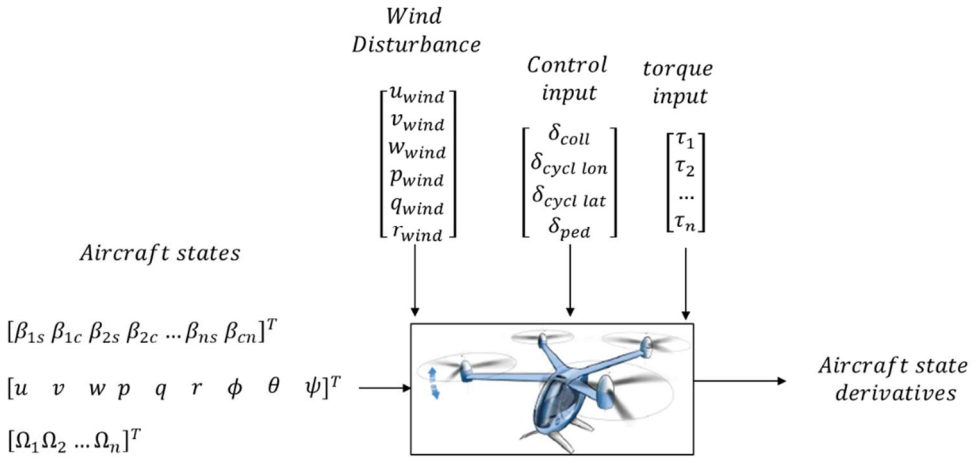

Figure 4 Schematic representation of the airframe dynamics

2. Controller Architecture

A robust control architecture is desired at the vehicle level to allow for stable flight. A Linear Quadratic Integral (LQI) control architecture can be leveraged as the baseline flight controller for the variable pitch quadrotor architectures [7]. The LQI control architecture is an extension of the Linear Quadratic Regulator (LQR) problem where an optimal state-feedback gain is determined that will achieve guaranteed robustness while minimizing energy spent [8]. The guaranteed robustness is achieved in the LQR problem by minimizing a quadratic cost function to regulate the states back to their equilibrium. In order to track non-zero states, as is desired in this application, the control law can be extended to facilitate integral based state tracking. The assumption was made that all necessary states are both available and observable to be used in the control architecture. The application of the linear optimal control architecture is considered a good match since the implementation of LQI control is relatively straightforward while the robust tuning process allows for a stable performance in diverse operating conditions.

The LQI problem can be defined as follows [1] by considering a linear, state-space dynamic system model:

$$\begin{aligned} \dot{x} &= Ax + Bu \\ y &= Cx \end{aligned} \tag{1}$$

Where, $x \in \mathbb{R}^n$ is the state vector, $y \in \mathbb{R}^q$ is the output vector, $u \in \mathbb{R}^m$ is the control input vector, $A \in \mathbb{R}^{n\times n}$ represent the system dynamics, $B \in \mathbb{R}^{n\times m}$ is the input matrix and $C \in \mathbb{R}^{q\times n}$ is the output matrix. The integrated error signal between desired tracking state reference values can be concatenated to the state vector x, where $\tilde{x} \in \mathbb{R}^p$:

$$z = \begin{bmatrix} x \\ \tilde{x} \end{bmatrix} \tag{2}$$

As shown in [1], an optimal state-feedback control gain matrix $K \in \mathbb{R}^{m\times(n+p)}$ can be synthesized such that state-feedback control law:

$$u = -K \begin{bmatrix} x \\ \tilde{x} \end{bmatrix} \tag{3}$$

minimizes the following cost function:

$$J(u) = \int_0^\infty [z^T Q z + u^T R u] dt \tag{4}$$

Where, $Q \in \mathbb{R}^{(n+p)\times(n+p)}$ is a diagonal tuning matrix where the terms represent a weighting factor for state diversion of vector z, and $R \in \mathbb{R}^{m\times m}$ is a diagonal tuning matrix where the terms represent a penalization of control action in u.

Figure 5 shows the application of the LQI control architecture to the variable pitch quadrotor vehicles. The reference tracking states of interest for the LQI collective pitch controller are the forward velocity in the inertial reference frame, $\dot{X}_{des}$, and the rate of climb in the inertial reference frame, $\dot{Z}_{des}$, both provided by the NDARC mission profile (Figure 1). All other states, that is the side velocity in the inertial reference frame (Y), the angular rates in the body reference frame (p, q, r), and the attitude angles (ϕ, θ, ψ), are regulated in steady-state (targeting zero), except for the pitch angle (θ) which in practice settles at a non-zero value during non-hover operations. Ω represents the motor RPM value for the n motors. The powertrain attempts to keep the RPM value constant between the motors in the collective pitch control vehicle. The wind disturbance acts as an external unknown disturbance to the system.

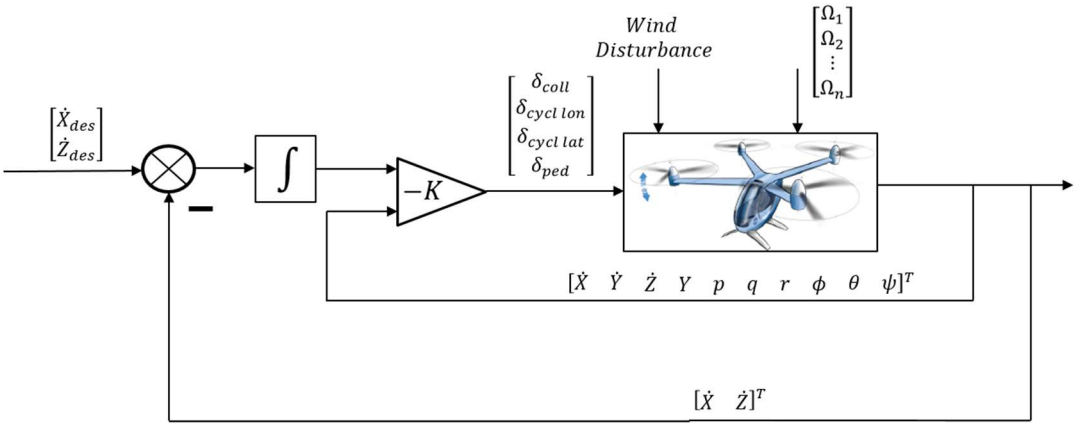

Figure 5 LQI control architecture applied to a variable pitch vehicle

3. Guidance and Navigation Module

The described LQI control architecture provides a stabilizing and robust control architecture for a set of reference states of interest. A guidance and navigation module is required in order to provide the reference states of interest such that the UAM mission in Figure 1 is followed by the vehicle. A high-level overview of the implemented guidance and navigation module can be seen in Figure 6. The NDARC mission profile was embedded into the guidance and navigation module as a set of desired inertial reference waypoints and velocities.

Current inertial reference coordinates are fed from the airframe dynamics module to the guidance and navigation module to determine where the vehicle is currently located with respect to the NDARC mission profile (Figure 1). The guidance and navigation module outputs a desired forward velocity and rate of climb defined in the inertial reference frame based on the NDARC mission profile and the location of the vehicle with respect to the next waypoint in the X and Z direction. Motion in the Y direction is not of interest as an output of the guidance and navigation module due to the inherent 2D definition of the NDARC mission profile and is therefore regulated (driven to zero). Additional tasks for the guidance and navigation module include accelerating or decelerating from or to hover, and timed hover maneuvers.

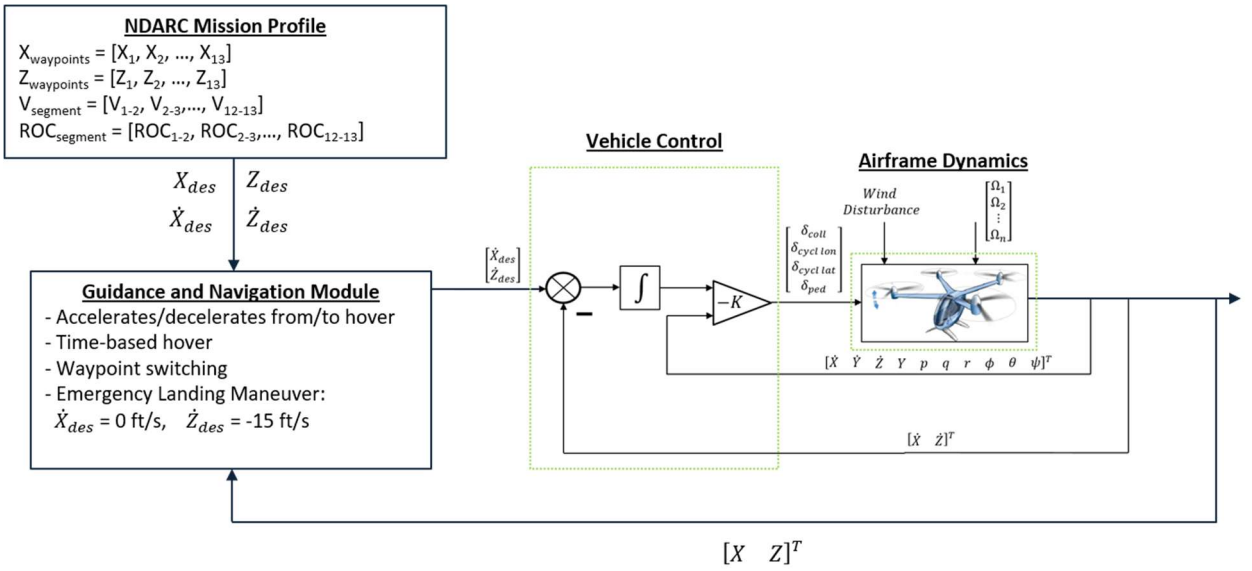

Figure 6 Guidance and navigation module

C. Transmission Modeling

The transmission systems of the selected quadrotor designs serve two fundamental purposes. First goal is reducing the higher rotational speeds of power generating components, such as electric motors and turboshafts, to the lower rotor rotational speeds. The second purpose is to provide alternative power supply paths (cross-shafting) to the rotors for safe flight if one of the turboshafts or electric motors fails. There is a need for cross-shafting because an unpowered rotor causes catastrophic failure for a quadrotor due to the loss of vehicle control.

On the other hand, the mechanical connections among the power sources create an opportunity for load sharing among the turboshafts or electric motors. The cross-shafting is engaged to the

Figure 7 provides the rotating component diagram for an electric quadrotor concept using collective control. The planetary gears between the electric motors and rotors reduce the rotational speed at the electric motor exit to the rotor rotational speed. This speed reduction is one of the two purposes of mechanical powertrain as stated earlier. The bevel gears between the electric motors and the planetary gears direct some of the electric motor power to a cross-shafting system which provides an alternative power supply path for all the rotors when one of the electric motors fails. This is the second listed purpose of a mechanical powertrain system. If a quadcopter rotor stops spinning in flight, such an event causes a catastrophic failure due to loss of control. Therefore, the cross-shafting system in Figure 7 is proposed to keep all the rotors powered when an electric motor fails.

Figure 8 shows the rotating components diagram for a series hybrid quadrotor with collective control. The mechanical powertrain in Figure 8 reduces the electric motor rotational speed to the rotor rotational speed with planetary gearboxes like the electric quadcopter in Figure 7. Moreover, the cross-shafting system in Figure 8 is the same as the system in Figure 7 and ready to provide alternative power paths when needed. The only difference between the quadrotor concepts in Figure 7 and Figure 8 is the turboshaft engine and the electric generator attached to the turboshaft. The series hybrid concept replaces most of the batteries in the electric quadrotor concept with a fuel tank for the turboshaft and generator couple for electricity production.

In contrast, Figure 9 introduces a different quadrotor concept with respect to the concepts in Figure 7 and Figure 8. The rotating components diagram in Figure 9 is for a collective control quadrotor with two turboshaft engines. The electric motors in the previous two concepts are replaced with two turboshafts. The power generated by the two gas turbines are blended with a series of gears. Then, the blended power is provided to each rotor through the central gearbox and the cross-shafts attached to the central gearbox. As the generated power is blended and transmitted, the rotational speed is reduced from the turboshaft rotational speed to the rotor rotational speed. If a power source fails, the failed gas turbine is disengaged from the powertrain with an overrunning clutch and the remaining gas turbine powers all the four rotors.

When the mechanical powertrain components in Figure 7, Figure 8 and Figure 9 are listed, it can be seen that there are only a few types of components. The types of mechanical components are shafts, bearings, gears and clutches.

The dominant transient mechanical components are the shafts with their rotational inertias, speeds and net torque calculations. The bearing inertias can be added to the shaft inertias and the frictional losses in the bearings can be represented with shaft transmission efficiency changes. The shafts were modeled as the only mechanical component with dynamic behavior in this work and the bearing inertias were neglected but the bearing losses were included in the transmission efficiency. The mechanical powertrain analysis assumes rigid components.

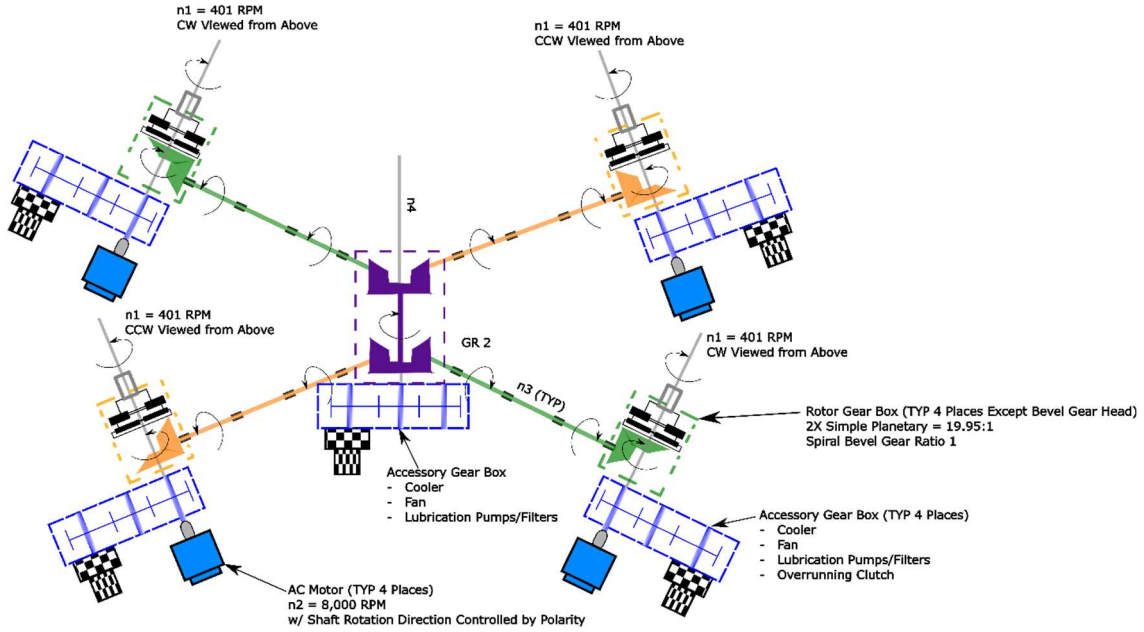

Figure 7 Electric collective control quadrotor rotating components diagram

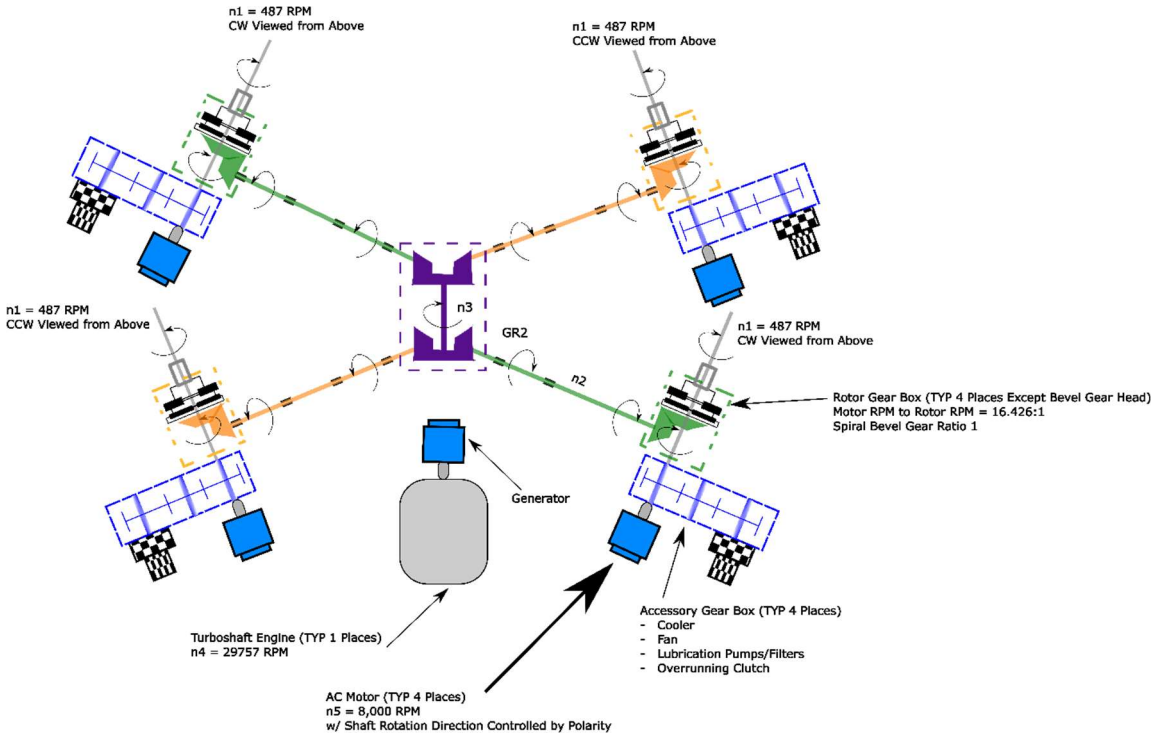

Figure 8 Series-hybrid collective control quadrotor rotating components diagram

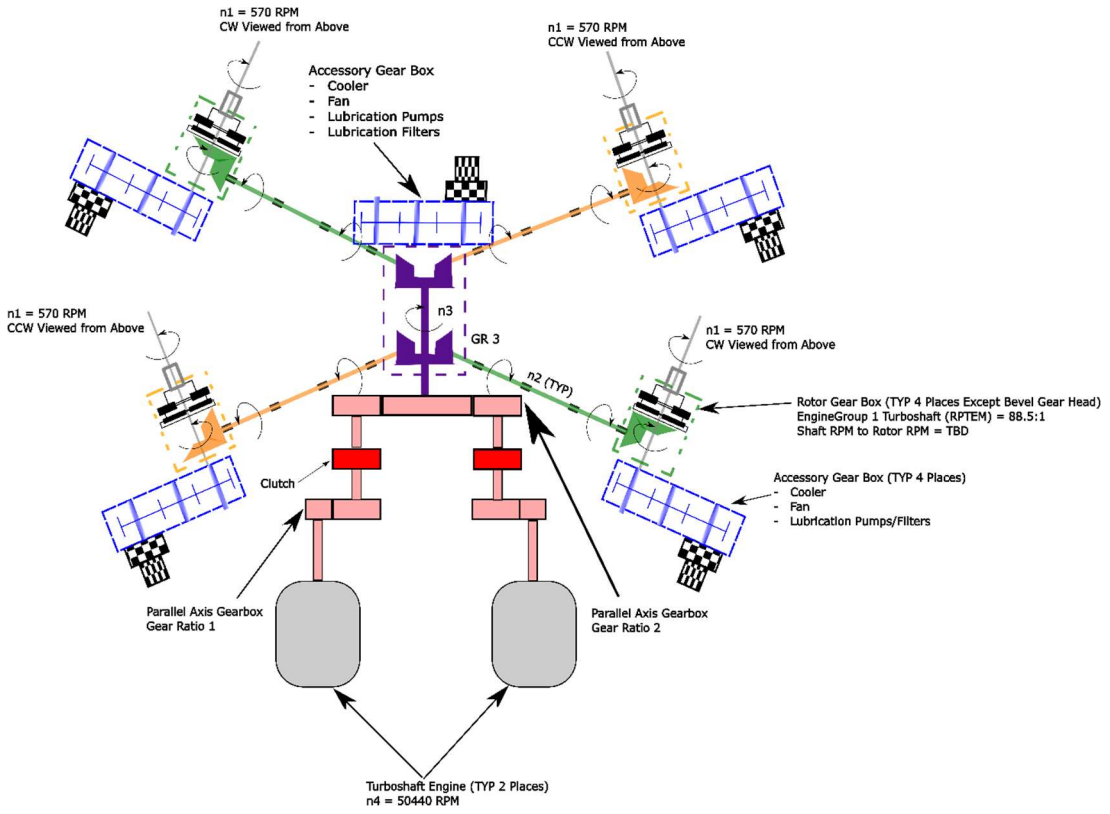

Figure 9 Conventional collective control quadrotor rotating components diagram

Like bearing inertia, gear inertias can also be added to the shaft inertias if needed as gears are important for dynamic mechanical simulations because they relate the gearbox inlet and outlet rotational speed, acceleration and torque values through their gear ratio. The gear inertias were neglected in this study, but the gear ratio-based speed, acceleration and torque relations were included.

Lastly, the clutch disengages the failed power generators like electric motors or gas turbines from the powertrain. The dynamic aspects of clutch engagement or disengagement are neglected but the effects of a disengaged clutch are modeled by setting the power input of an electric motor or gas turbine equal to zero.

D. Turboshaft Modeling

Two transient two-shaft turboshaft Numerical Propulsion System Simulation (NPSS) models are developed for the simulation environment. The first one is a turboshaft model for the series-hybrid quadrotor concept and it generates a Maximum Rated Power (MRP) of about 950 hp in Sea Level Static (SLS) conditions. The second one is a turboshaft model for the quadrotor concept and supplies a MRP of 450 hp in SLS conditions. The conventional and series hybrid quadcopter concepts have different numbers of turboshafts: while the conventional quadcopter concept has two gas turbines, the series hybrid quadcopter concept has a single gas turbine.

The two transient turboshaft models developed as part of this study feature spool dynamics. Spool dynamics is the fundamental gas turbine dynamics because the spool dynamics captures the interactions among the power consuming and producing gas turbine components on a spool. Without the net power calculation for a spool, the transient gas turbine model cannot predict steady state performance let alone transient performance. Therefore, every transient gas turbine model has spool dynamics.

Modeling spool dynamics require spool rotational inertia values. It is beyond the scope of this paper to develop a gas turbine weight prediction model like a WATE++ model [9]. Therefore, the spool rotational inertia values are determined by calibrating for the typical spool dynamics time constant values provided in the literature. The typical time constant value for spool dynamics is about one second.

The other gas turbine dynamics are volume dynamics, heat soak effects and tip clearance effects. Volume dynamics is the accumulation of gas mass inside the cavities in the gas turbine components. Volume dynamics is the fastest dynamics in a gas turbine but modeling volume dynamics is necessary if the goal is to analyze high frequency events like stall or the gas turbine model has a large enough volume that can slow down volume dynamics enough to affect spool dynamics. In this paper, the goal is not to study stall or the modeled turboshaft engines do not have a large internal volume. Therefore, volume dynamics is not simulated in the developed models.

Heat soak effects are the heat transfers between a component's material and the flow going through the component during operation. Simulating heat soak effects require a basic component geometry and weight information, but such information was not available because it was outside the scope of this paper to develop a weight model like WATE++. Therefore, heat soak effects were not included in the developed transient turboshaft models either.

Tip clearance effects depend on the spool dynamics and heat soak effects. The spool dynamics determines the pull forces on the turbomachinery blades as a function of spool speed. The blade strains change as the spool speed changes. On the other hand, heat soak effects provide the component material temperature changes which are necessary to calculate the subcomponent thermal expansions or contractions. Tip clearances are computed from the blade strains and overall thermal size changes. The developed model does not include tip clearance effects because heat soak effects are not included as a result of unavailable basic component weight and geometry.

Although nonlinear transient turboshaft NPSS models were developed, the linear models were generated from the developed NPSS models across the flight envelope. The generated turboshaft linear models were integrated with the simulation environment in MATLAB. Using the linear models prevents the computation overhead of integrating the MATLAB environment with NPSS. Moreover, the imported linear models can be used with the functionality in MATLAB unlike an external function call to NPSS. In particular, the generated linear models can be used with the control functions in MATLAB.

The created linear turboshaft models were scheduled across the flight envelope based on the flight condition and power setting. To control the power turbine rotational speed, a Linear Quadratic Regulator (LQR) controller design was used as the turboshaft speed governor. The scheduled linear turboshaft models represented the turboshaft dynamics for the LQR process.

E. Electric Propulsion Systems Modeling

Two of the three analyzed quadcopters in this paper are equipped with electric powertrains and a lithium-ion Battery Pack (BP). Every electric powertrain consists of an Electric Motor (EM) and the related Electronic Speed Controller (ESC). In particular, Permanent Magnet Synchronous Motors (PMSMs) are selected due to their high

energy density and low inertia compared to the other electric machines [9], while the ESC is based on a three-phase voltage-controlled inverter. The ESC has the function of:

i) providing the EM with the proper voltage to achieve the desired torque reference through PI controllers.

ii) enforcing the power limits of EM (continuous and peak operation) and BP ensuring the operation of the system within the components' safe operating area.

Figure 10 represents the logic of the dynamic model of the electric propulsion system, in which all the main components have been modeled and the control strategy has been illustrated. In detail, the PMSM is modeled using a *d-q model* in which the dynamic of the d-axis has been ignored for simplicity. This is a good approximation for system level analysis and when surface mounted PMSM are considered, with the advantage of reducing the computational complexity of the model. Moreover, this approximation ignores the flux dynamic during the field-weakening operation. This approximation will not affect torque availability, efficiency, and fault modes. In addition, it is worth mentioning that the considered d-q model neglects field saturation, eddy currents and hysteresis losses of EM, considers sinusoidal induced ElectroMotive Force (EMF), no field current dynamics and damper winding [10]. The ESC voltage dynamic due to the modulation technique is ignored as well due to the fast time constant when compared to the overall vehicle simulation. The efficiency of the EM and ESC are combined in the efficiency map reported in Figure 11. Depending on the size of the propulsion system the efficiency map is scaled up or down to satisfy the vehicle requirements [11].

The motor control strategy is based on the torque request defined by the master-slave rotors controller with the aim of achieving the desired vehicle speed and position. The torque request is converted to q-axis current request (i_q^{**}) and saturated considering the Intermediate Rated Power limit (IRP, red line, maximum application 30 minutes) and the Maximum Continuous Power limit (MCP, black line) defined for each torque-speed combination, as shown in Figure 11. In addition to the motor power limit, a current rate limiter is also applied to constrain the rate of change of i_q^{**}. The motor control strategy is based on a Field Oriented control (FOC). A PI controller is used for deriving the q-axis voltage (v_q) for the EM, given the saturated i_q^* and the actual q-axis current (i_q).

For the battery pack, a zero-order model is considered according to the specifications reported by NDARC ([5], [12]). This model considers both current and temperature effects on the battery pack parameters. The battery power request is calculated as the summation of all the requests from the electric powertrains, as function of i_q, motor speed, EM and ESC efficiencies. The battery pack power limits are calculated considering the maximum C-rate allowable and applied to constrain the electric motor power consumption as well [13] .

A lumped-parameter thermal model of EM and ESC is included as well for evaluating the thermal performance of the electric powertrain in case of air or liquid cooling. The proposed model is then calibrated using the NDARC specification [5] and considering the vehicle specifications (e.g. one motor inoperative condition). A summary of the design parameters is included in Figure 11.

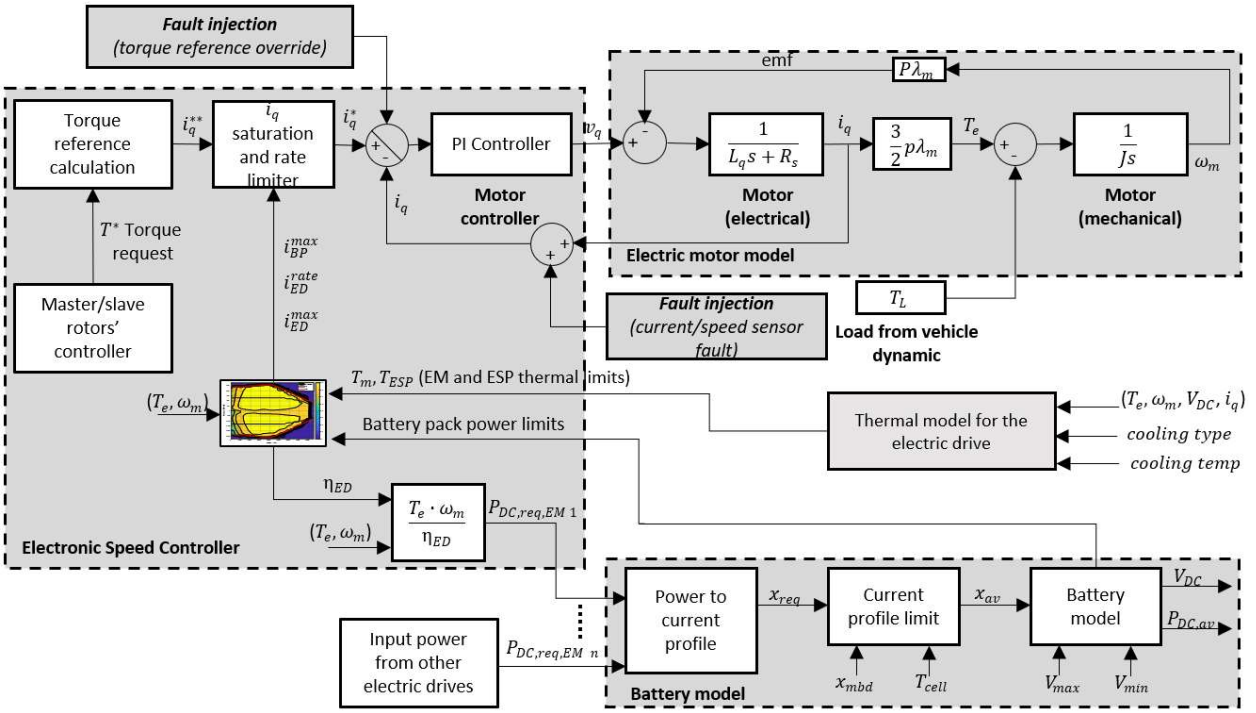

Figure 10 Block diagram of the dynamic model of the electric propulsion system

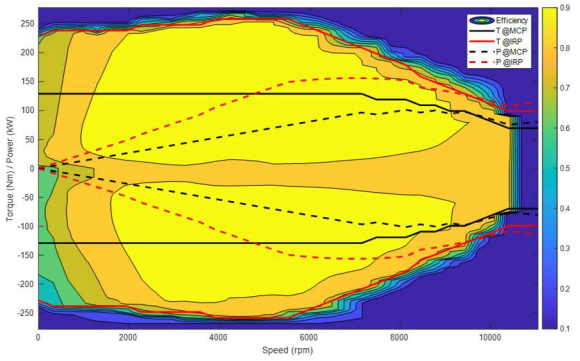

Architecture	Design	SLS MCP @8krpm	SLS IRP @8krpm	ESS sizing
Quadcopter electric	NDARC	112hp 83kW	168hp 125.3kW	552kWh
	GT-OSU	88.5kW	137kW	
Quadcopter hybrid	NDARC	66.6 hp 50kW	100 hp 75kW	83.4kWh
	GT-OSU	64kW	99kW	
	NDARC generator	472.78hp 352.55kW	709.18hp 528.83kW	

Figure 11 Example of electric motor efficiency map and table including the electric drive design parameters

F. Speed Control

The quadcopters with electric motors (all electric and hybrid) have a mechanical coupling link between the rotors (cross-shafting). This poses a problem for speed control, as the electric motors have to collaborate, or share the torque required. The proposed strategy is to have one of the motors designated as a master, which operates in speed control, and the other rotors to operate as followers, in torque control. The master regulates the angular velocity, and the followers follow the current of the master.

When one of the motors presents a fault, the master-follower approach can present the danger that all motors could be affected by the consequences of that fault. In order to limit this effect, the following rules were implemented in the angular motor control loop:

- A motor with an electric fault or malfunction cannot be a master, and becomes a follower
- If a mechanical linkage breaks and a motor is isolated from the other ones, this motor operates in speed control on its own, not as part of the master-follower algorithm

For the configurations with mechanical links between the rotors, it is not possible to apply individual speed control approach. Consequently, a master-follower controller is used to control the multiple electric motors of the electric and hybrid quadrotor vehicles. This approach consists in having one motor operating in speed control (master), and the other motors (followers) are matching the current of the master motor. The current desired is an output of the speed control PI loop of the master motor. It is used by all the motors, as shown on Figure 12. Because the motors are attempting to operate with the same current, they provide the same torque, which leads to a uniform use of the different motors. In the nominal configuration, no logic is used to select the master motor, and the master motor is motor number 1.

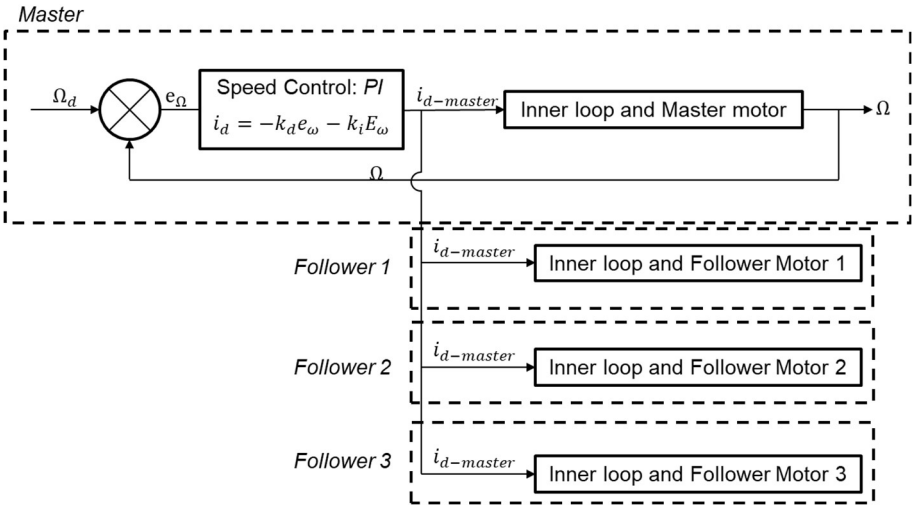

Figure 12 Master-follower approach

In a case of motor or transmission malfunction, the master-follower approach is modified. First, if the Motor 1 has a malfunction, the master control is assigned to another motor, typically Motor 2, as shown in Figure 13. It is important to note that this implementation requires the identification and diagnosis of motor malfunctions.

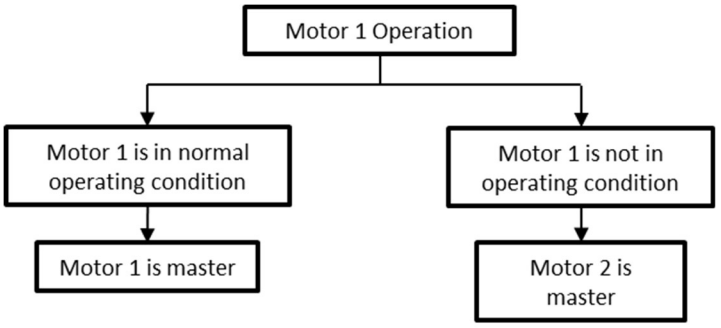

Figure 13 Master assignment when motor 1 has a malfunction

Second, if the transmission (cross shafting) fails and a rotor is isolated, this motor will operate on its own speed control loop. The other motors are kept in master-follower control, as shown on Figure 14. Once again, it is important to note that this implementation requires that it is possible to diagnose a transmission and motor malfunction.

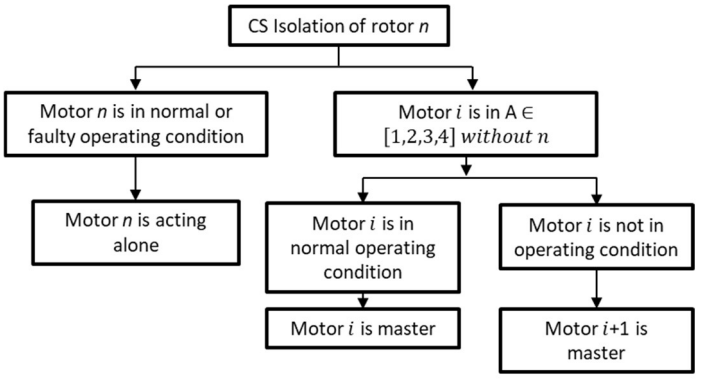

Figure 14 Master control assignment after isolation of motor *n*

IV. Fault Modeling

A. Transmission Faults

The developed simulation environment includes failure modes for the elements used in the mechanical power transmission systems. The element types in the mechanical power transmission systems are shaft, bearing, gear and clutch. The simulated component failure modes are not comprehensive but provide a large enough set for various failure scenarios.

The shaft elements can break due to overloading or fatigue in transient simulation [14, 15, 16]. When a shaft is overloaded, the shaft experiences a single load which surpasses its yield or tensile strength the instant before the failure. An uncontrolled increase in the load on the shaft can be due to an emergency demand or control system failure. A shaft fracture due to fatigue occurs suddenly due to a slow crack growth as a result of many rotations under load. The crack forms in the shaft due to a manufacturing defect, corrosion or a damage caused during or before operation. When fractured, a shaft element transmits no power and that is how the shaft break is modeled.

In a vehicle concept, fractures of different shaft components have different effects. For instance, the fracture of one of the cross-shafts in the electric quadrotor concept in Figure 7 isolates one of the electric motor-rotor pairs from the rest of the cross-shafting system. The quadrotor can continue to operate without any immediate problem if the isolated electric motor does not fail. On the other hand, breaking one of the rotor shafts stops the power transmission to that rotor. For a quadcopter, an unpowered rotor is a catastrophic failure due to the loss of vehicle control.

The failure modes for a bearing element are spalling and fracture [17, 18]. Spalling is bearing surface irregularities which increases friction and vibration. Subsurface or surface-initiated fatigue due to reaching the end of life, wear, corrosion, contamination, or overheating causes spalling. On the other hand, a bearing fractures when one or more of the bearing components such as cage, inner and outer rings breaks. The bearing fracture occurs when the strength of the material is exceeded due to overloading or the fatigue limit of the material is exceeded under the given operating condition.

Spalling is modeled as a decrease in component power transmission efficiency because of the increase in bearing friction and vibration after spalling. However, a bearing fracture is modeled like a shaft break because a shaft can be dislocated after a bearing fails. A dislocated shaft fails to transmit power in the same manner as a broken shaft.

The modeled gear failure modes are teeth surface failures and tooth fracture due to fatigue or overloading [15, 19, 20]. The teeth surface failures consist of gear failures such as surface material fatigue such as pitting and spalling, wear and plastic deformation or flow. The teeth surface failures decrease the transmission efficiency and increase vibration. Therefore, the teeth surface failures are modeled as decreases in component efficiency. On the other hand, tooth fracture due to fatigue is a result of reaching the fatigue life limit for the gear. Like the other components, gear tooth fracture due to overloading occurs when a load larger than the gear's material strength is applied to the component. Gear tooth fractures are modeled as severe component efficiency reductions.

The last mechanical powertrain component type is the overrunning clutch [21, 22, 23]. Three failure modes are modeled for the clutch element. The simulated clutch failure modes are fracture due to overloading or fatigue and degradation. The clutch elements fracture due to overloading when the clutch experiences a load larger than its material strength. Like the other components, a clutch element also breaks when the clutch reaches its fatigue life limit. When broken, the clutch is assumed to be incapable of engaging. Thus, the power source connected to the failed clutch, such as an electric motor, is disengaged from the powertrain. The model sets the power input from the

disengaged power source equal to zero to simulate overrunning clutch fractures. On the other hand, the clutch experiences deterioration due to freewheeling, differential speed and shock loads in clutch engagements, and disengagements at high speeds. The clutch degradation is modeled as component efficiency loss.

B. Turboshaft Faults

The simulated turboshaft faults are recoverable and non-recoverable failures [24, 25]. The recoverable turboshaft failures are adverse events which interrupt turboshaft performance for a short duration such as single or multiple stalls, flame-out, bird ingestion and Foreign Object Damage (FOD). On the other hand, the non-recoverable turboshaft failures are severe damages which prevent the flight crew from restarting the turboshaft.

The non-recoverable turboshaft failures are modeled by setting the power generated by the failed turboshaft equal to zero. On the other hand, the recoverable turboshaft failures are simulated by setting the failed turboshaft power generation equal to zero for a short duration. As a side note, the turboshaft model is not capable of simulating the short transients between the fault occurrence and the power loss. Therefore, the power generation is set to zero directly when the fault is introduced.

C. Electric Systems Faults

The model described in Section III.E is then equipped with dynamic models of the electric propulsion system faults with the aim of evaluating the overall system reliability using Dynamic Event Tree (DET). Considering the Fault Tree Analysis (FTA) and Failure Mode, Effects & Criticality Analysis (FMECA) process proposed in [3] the fault models have been integrated in the electric powertrain model, as shown in Figure 10.

A multitude of faults can happen in EM, ESC, electronic power distribution and lithium-ion batteries [26] [27]. For example, in this work the impact of voltage and current levels, thermal stress due to different thermal management solutions, potential failures due to overcharge, overdischarge and high c-rate operation have been investigated among others. Examples of FTA and FMECA of components of the electric propulsion system are reported in [26] [27]. It is clear that the development of accurate models of all the possible faults that can occur in an electric propulsion system can be necessary for accurate reliability analysis, however the results of the DET [4] may be difficult to comprehend and analyze at the system level in such a case. For this purpose, the faults were categorized based on their effects on the powertrain as reported in .

1. **No torque** – For example, this condition can be observed in case of complete failure of the cooling system for ESC, EM, or battery pack. The shutdown due to overtemperature causes no torque output for the Electric Drive (ED).
2. **Low torque** - Internal battery failure (such as cell short circuit) is one such example case, that can lead to a low torque output for the ED due to lower voltage or capacity.
3. **Torque ripple** – A fault in the current or speed sensor of the powertrain can lead to oscillation in the torque output while the average torque still meeting the torque request.
4. **High torque** – An electric distribution failure due to failure-to-open of a contactor can cause a high torque output for the ED.
5. **Short circuits modes:** Three short circuit modes are considered to take into account for single phase, two-phase, three-phase short circuits and including the response of the ESC.
    - **Mode 1 - Torque transient** – After a short circuit, the ESC or the vehicle supervisory control may turn-off the ED causing the high torque condition to be eliminated.
    - **Mode 2 - High torque oscillations** - This condition is observed when short circuit occurs in EM winding or ESC.
    - **Mode 3 – Dumped torque oscillations** - This condition is observed when short circuit occur in EM winding or ESC.

Table 3 Failure modes and causes defined for all the main components of the electric system

Failure Mode	*No torque*	*Low torque*	*Torque ripple*	*High torque*	*Short circuit modes 1,2,3*
Failure Cause	30% Rotor failure - total demagnetization 30% Mechanical failure ESC, EM, or BP cooling failure - shutdown due to overtemperature 70% Electric distribution failure (open contactor, burn fuse, connections) ESC controller failure except inverter or DC capacitor short circuit BMS failure 30% Cell external short circuit 30% Cell internal short circuit	70% Rotor failure - partial demagnetization 70% Mechanical failure DC capacitor open circuit EM, ESC, BP reach warning temperature – ESC derating 70% Cell internal failure 70% Cell external failure	Current sensor fault Speed sensor fault EM winding or Invert open phase fault	30% Electric distribution failure (close contactor, short connection)	EM winding short circuit (single phase, bi-phase, three phase) and ESC short circuit (inverter or DC capacitor) EM and ESC turn off due to vehicle supervisory controller request

reports the details of the categorization based on an extensive literature review as well as simulations. Then, the fault models have been integrated in the electric powertrain model. Figure 15 shows the different torque and q-axis current profiles that can be achieved by injecting faults in the electric powertrain model (Figure 10), highlighting the corresponding class of effects, including no torque, low torque, high torque, torque transient, torque ripple and high torque oscillations due to short circuit. Both the magnitude and the time injection can be set as desired.

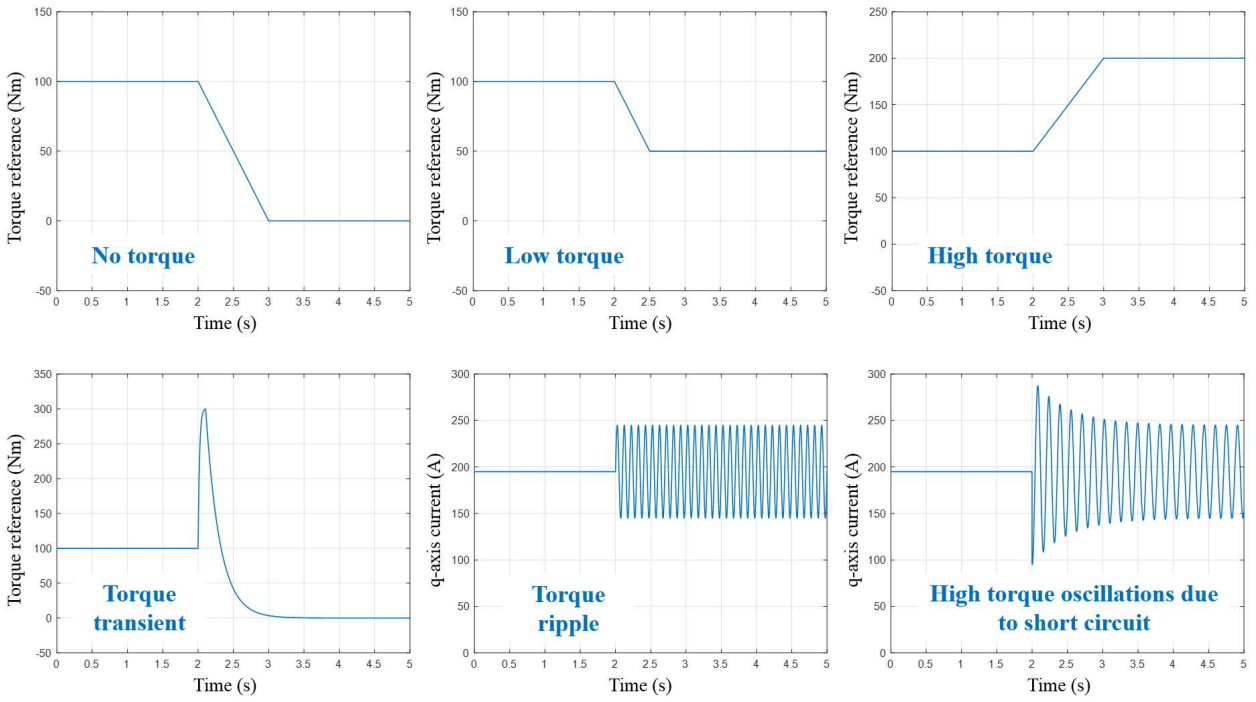

Figure 15 Different torque and q-axis current by injecting faults in the electric powertrain model.

V. Simulation Results and Test cases

A. Nominal Flight of the Electric Quadrotor

Figure 16 through Figure 19 show nominal mission characteristics for the quad electric vehicle. To shorten simulation time, only the second leg of the defined NDARC mission profile (Figure 1) is simulated. Figure 16 shows the body frame velocity components on the left and the translational displacement profile on the right. As can be seen, the vehicle follows the NDARC design mission closely with the desired vertical and horizontal velocities. The timed hover sections can be seen as well. Figure 17 shows the smooth angular velocity and displacement profiles. Figure 18 shows the rotor angular velocity and electric machine power profile. The angular velocities of the four rotors are equal to each other, as is expected due to the cross shafting, and the magnitude is mostly constant if not for some small magnitude excursions during transient flight phases. The electric machine power profile shows that all four motors are well below the IRP and only cross the MCP during the take off and climb section. Figure 19 shows the motor torque and RPM overlaid on top the electric motor efficiency heat map. and the battery-related metric profile. Like Figure 18, the heat map shows that the torque limit approaches but does not cross the limit, and that the angular velocity of the motor stays constant throughout the nominal flight. The battery model shows a relatively linear discharge of the battery with the battery operation staying within the defined power limit.

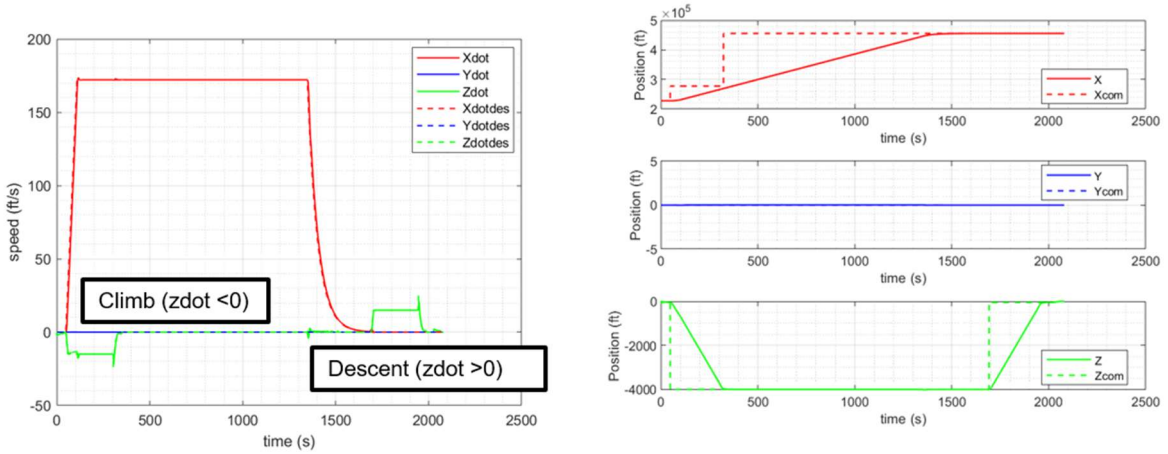

Figure 16 Quad electric nominal translational velocity profile (LEFT) and translational displacement profile (RIGHT)

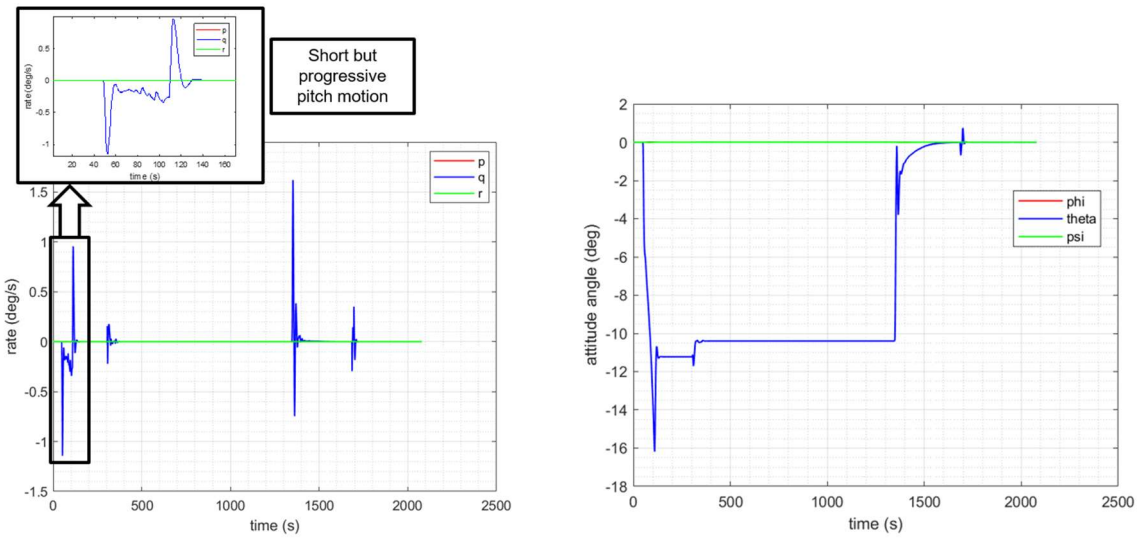

Figure 17 Quad electric nominal angular velocity profile (LEFT) and angular displacement profile (RIGHT)

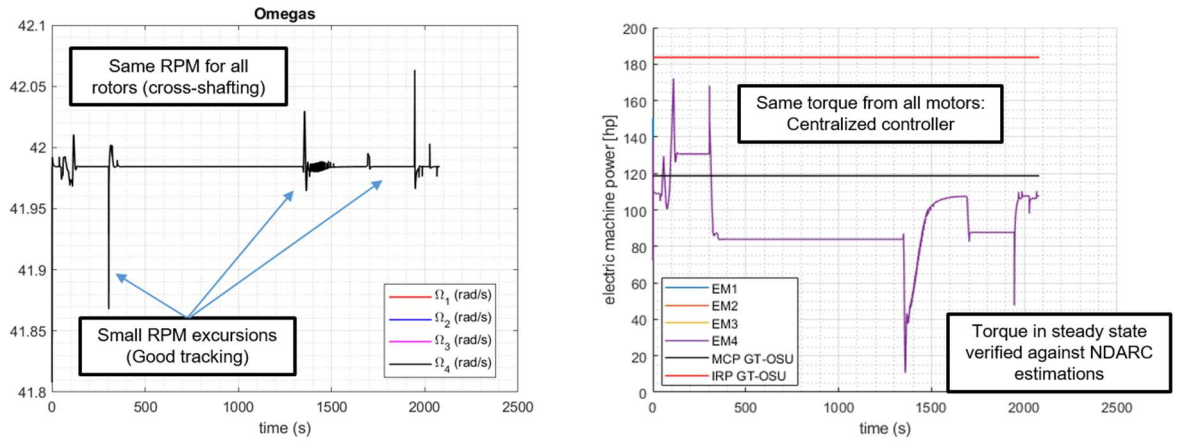

Figure 18 Quad electric nominal rotor angular velocity (LEFT) and electric machine power profile (RIGHT)

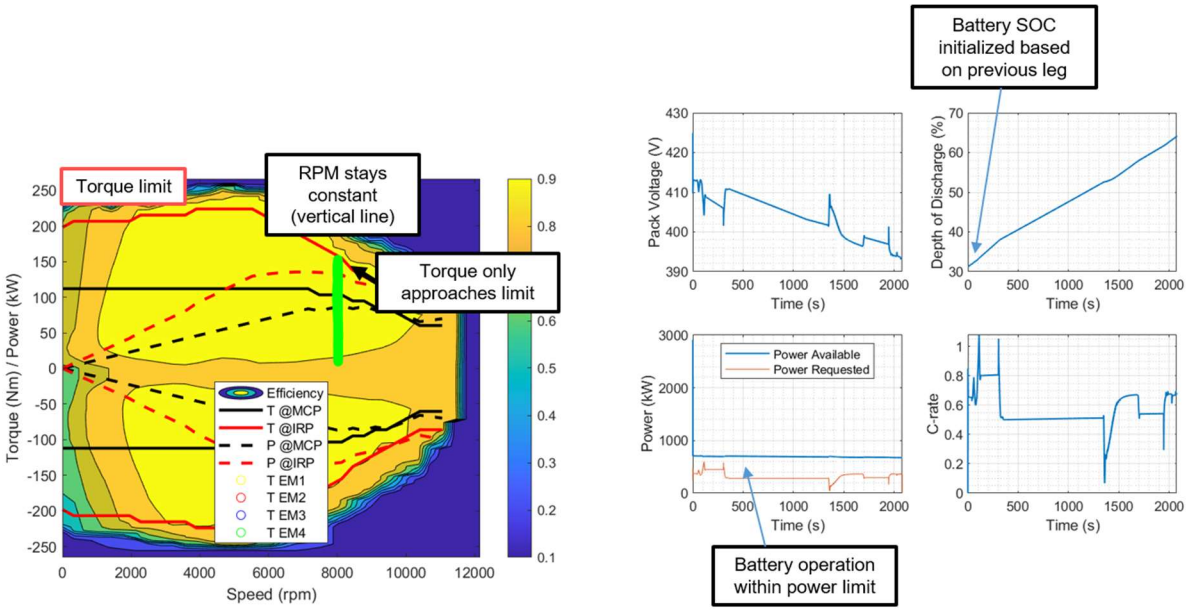

Figure 19 Quad electric heat map (LEFT) and battery profile (RIGHT)

B. Nominal Flight of the Series-Hybrid Quadrotor

The translational and rotational displacements and velocities for the nominal flight of the series-hybrid quadrotor look similar to those shown for the electric quadrotor vehicle in Figure 16 and Figure 17. The hybrid vehicle cruises at a higher cruise speed than the electric quadrotor vehicle. The turbine output during the flight can be seen in Figure 20. Figure 21 shows the rotor angular velocity and the electric machine power profile for the hybrid vehicle. Figure 22 shows the efficiency heat map and the battery characteristics. Per the defined task of the battery for the series-hybrid configuration by the NDARC design, the battery only aids in the flight phases where the power demand is high. This can be seen in Figure 22 where the battery power is used during take-off and hovers.

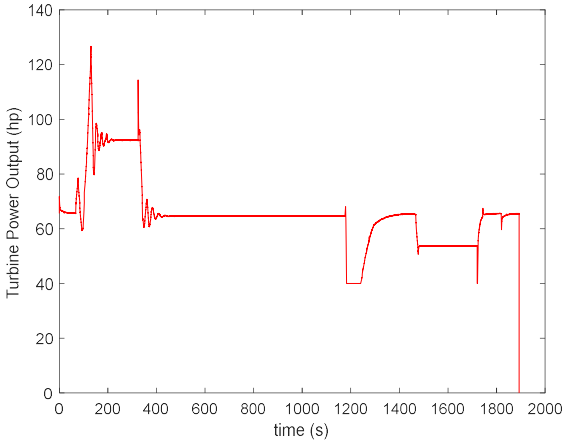

Figure 20 Turbine power output

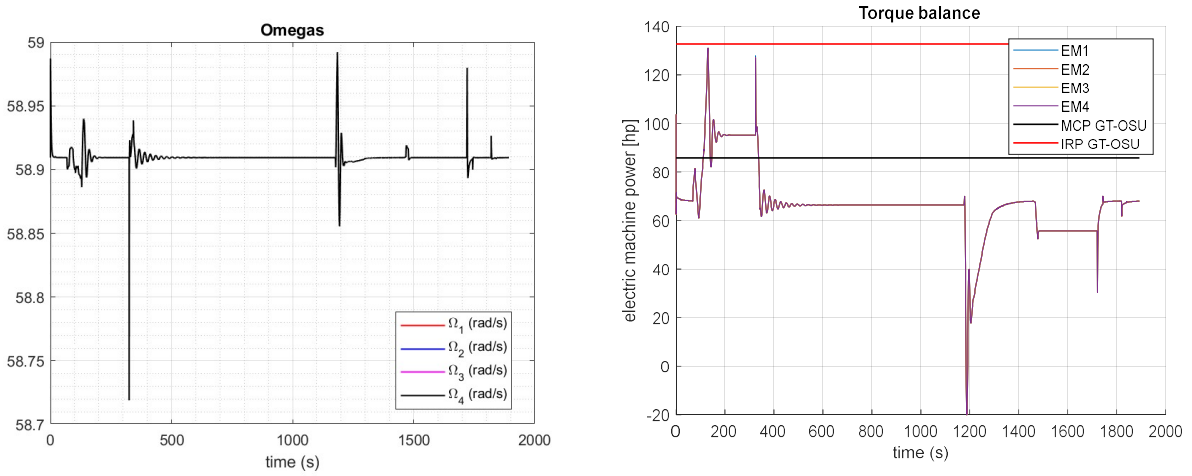

Figure 21 Quad hybrid nominal rotor angular velocity (LEFT) and electric machine power profile (RIGHT)

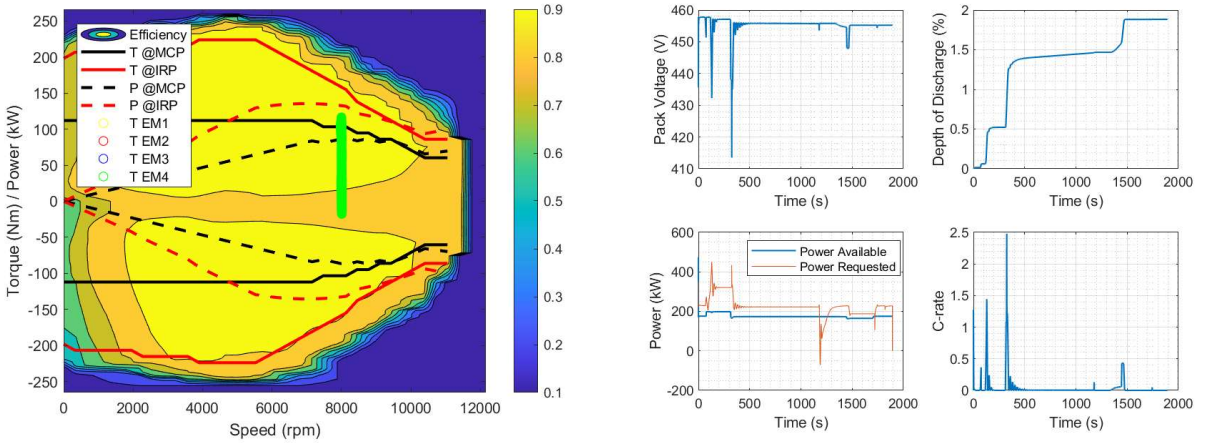

Figure 22 Quad hybrid heat map (LEFT) and battery profile (RIGHT)

C. Nominal Flight of the Turboshaft Quadrotor

The translational and rotational displacements, and velocities for the nominal flight of the turboshaft quadrotor also look similar to those shown for the electric quadrotor vehicle in Figure 16 and Figure 17. Like the hybrid vehicle, the turboshaft vehicle cruises at a higher cruise speed than the electric quadrotor vehicle. Figure 23 shows a time history of the turboshaft turbine power output and spool speeds. The low pressure and high-pressure spool speeds, and the power output of the turbine are expressed as a function of time. The low-pressure spool, the spool from which the power is extracted, stays relatively constant throughout the mission, while the high-pressure spool speed changes with the changes in power demands. It is important to note that the power output of the turbine is for one turbine only, and consequently, the power output of the combined turbines is twice as much. Given that the aircraft is performing only a longitudinal acceleration and that no wind is present, the lateral dynamics was omitted from the simulation.

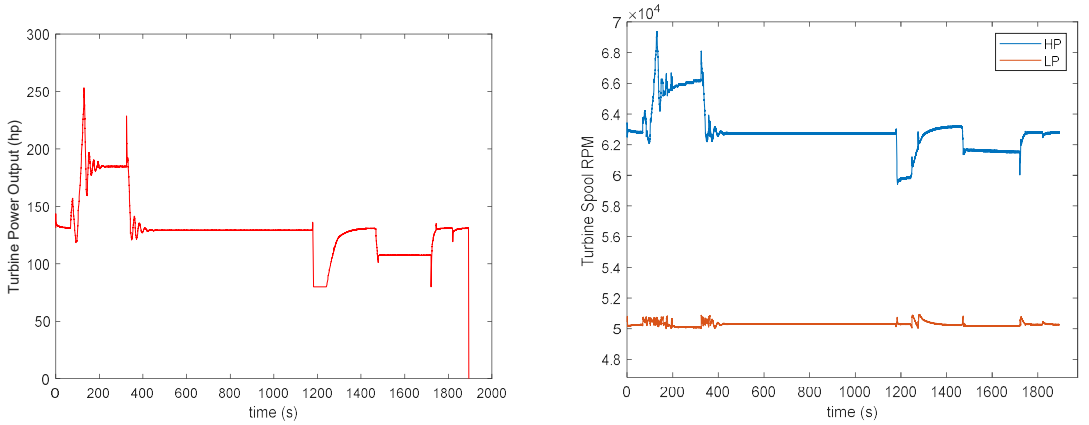

Figure 23 Quad with turboshaft power output (LEFT) and turbine Spool Speeds (RIGHT)

D. Electric Motor Fault

Figure 24 illustrate the simulation results of the electric quadcopter in hover while a no-torque fault occurs on Motor 1 at time t=200s. Given the presence of cross shafting and the reconfiguration of the master-follower approach once the fault is detected, the remaining three motors provide the lost torque. This reaction is fast enough to keep the loss of angular velocity below half a percent, as seen on Figure 24 (right). The no-torque fault applied on a single motor does not lead to a catastrophic event, and the mission can continue as planned.

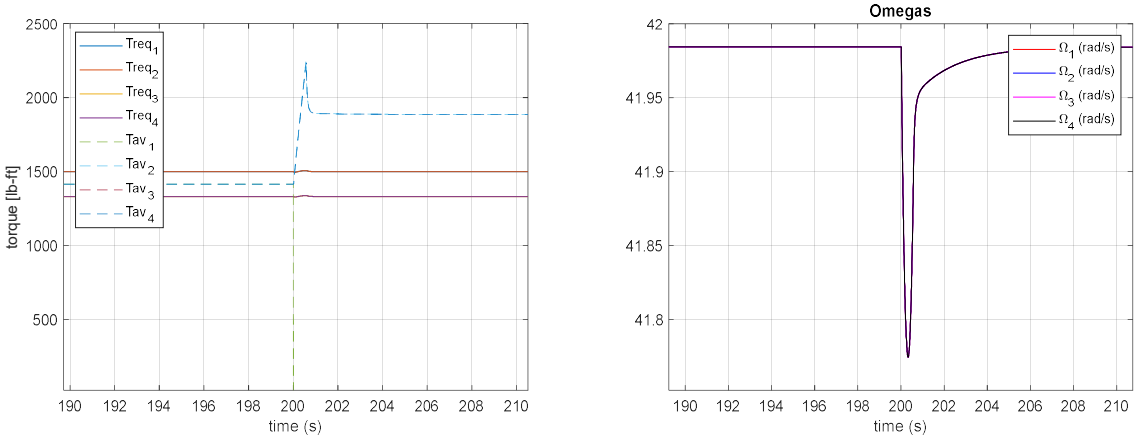

Figure 24 No torque fault applied on the Motor 1 of the electric quadrotor in hover. Torque balance (left) and angular velocity of the four rotors (right).

E. Electric Motor Isolation

For the electric-powered aircraft, the multiple rotors are mechanically coupled together to provide the ability to operate if one of the motors has a fault. As discussed in the previous sections, the master-follower approach is used to control the motors together. In the event of a rotor isolation, the control is reconfigured so that the isolated rotor operates on its own and the rotor still coupled continues to operate with the master-follower approach. The case of a rotor isolation in hover is explored and the results of a rotor isolation is shown on Figure 25. The aircraft is operating in hover, and at time t=10s, Rotor 1 is isolated. The power, which is uniform across the 4 motors until the isolation, is now slightly unbalanced, given that the front rotors need more torque in hover due to the center of gravity location. The motors 2, 3 and 4 keep operating at a uniform and constant power after the fault.

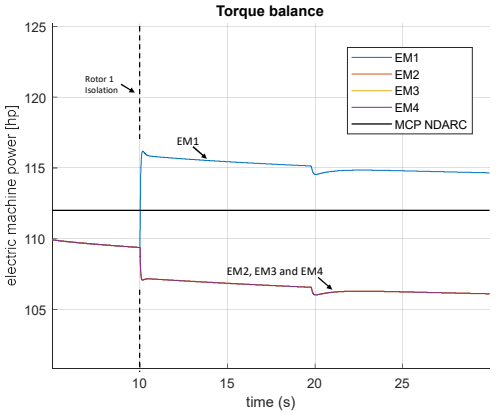

Figure 25 Torque balance in hover following a motor isolation

F. Turboshaft Fault

As discussed in the previous section, the turboshaft-equipped quadrotor has two turboshafts operating in parallel for redundancy. To gain insight into the system performance, the dynamic simulation of the two engines is carried out on Figure 26. The aircraft is operating in hover, and at time t=10s, a complete failure is simulated for one of the two turboshaft engines. At this point, the remaining turboshaft provides all the power needed to sustain the flight. The figure illustrates the high-pressure and low-pressure spool speeds of the operating turbine. It can be observed that at the time t=10s, there is a dip in the low-pressure spool speed, indicating a dip in rotor RPM, given that the low-pressure spool is connected to the rotors. The high-pressure spool sees an increase in RPM due to the increase in fuel flow rate to provide the additional torque. It is important to note that the transient dip in low-pressure spool speed is 2,550 RPM which is less than 5% of the nominal spool speed. The magnitude of the transient dip is relatively small and has limited impact on the vehicle motion.

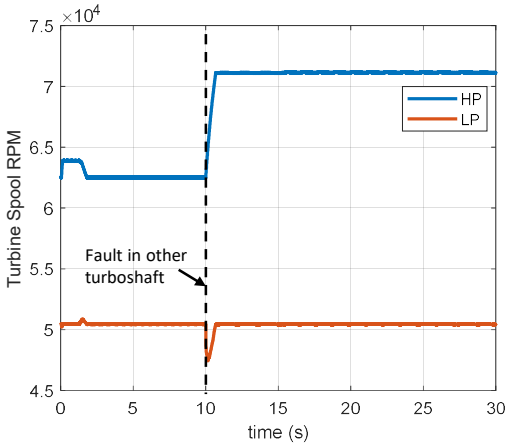

Figure 26 Turbine spool dynamics in hover following the loss of power in one turboshaft

VI. Conclusion

This paper presented the simulation environment developed to perform dynamic safety assessments of multicopter concepts. The discussion focused on quadrotors with three different propulsion architectures: electric, series-hybrid electric, and a turboshaft driven concept. The use of subsystems and component-based dynamic models allowed for the analysis of relevant fault mode impacts and the assessment of the transient vehicle response to both subsystem faults and longitudinal maneuvers. The nominal simulation results for the entire mission are illustrated, as well as the transients following an electric motor fault in hover. Additional results are shown for electric motor isolation in the electric quadcopter and a complete turboshaft fault in the turboshaft-driven quadcopter. The developed simulation environment is going to be used in the second phase of the effort, which consists of assessing the aircraft reliability and safety.

Acknowledgments

This research was supported by NASA Ames Research Center under contract NNA15AB13B, Task Order 80ARC020F0055, and titled “Reliability and Safety Assessment of Urban Air Mobility Concept Vehicles”. The authors would like to acknowledge the valuable feedback received throughout this research from Curtis Hanson, Robert Kufeld, Carlos Malpica, and Wayne Johnson.

VII. References

[1] W. Johnson, C. Silva and E. Solis, "Concept vehicles for VTOL air taxi operations," in *AHS International Technical Meeting on Aeromechanics Design for Transformative Vertical Flight*, 2018.

[2] P. R. Darmstadt, R. Catanese, A. Beiderman, F. Dones, E. Chen, M. P. Mistry, B. Babie, M. Beckman and R. Preator, "Hazards Analysis and Failure Modes and Effects Criticality Analysis (FMECA) of Four ConceptVehicle Propulsion System," NASA Technical Report, 2019.

[3] E. Li, S. Patel, M. D'Arpino, M. Ozcan, J. Gladin, C. Justin and D. Mavris, "Safety Assessment of the Novel Distributed/Hybrid Electric Propulsion Architectures for the Urban Air Mobility Vehicles," in *ANS PSA 2021*, Columbus, OH, 2021.

[4] G. Sarici Turkmen, T. Aldemir, S. Patel, M. D'Arpino, E. Demers Bouchard, J. Gladin and C. Justin, "Quantification of mission reliability for urban air mobility quadcoper using dynamic event trees," in *ANS PSA 2021*, Columbus, OH, 2021.

[5] W. Johnson, "NASA Design and Analysis of Rotorcraft (NDARC) - Theory," NASA Ames Research Center, Moffet Field, 2019.

[6] B. Lawrence, B. Lawrence, M. B. Tischler, C. R. Theodore, J. Elmore, A. Gallaher and E. L. Tobias, "Integrating Flight Dynamics & Control Analysis and Simulation in Rotorcraft Conceptual Design," in *AHS 72ndAnnual Forum*, West Palm Beach, 2016.

[7] P. Young and J. Willems, An approach to the linear multivariable servomechanism problem., 1972.

[8] W. S. Levine, The Control Handbook; Control system Advanced Method, Boca Raton: CRC press, 2011.

[9] J. De Santiago, H. Bernhoff, B. Ekergård, S. Eriksson, S. Ferhatovic, R. Waters and M. Leijon, "Electrical motor drivelines in commercial all-electric vehicles: A review. ," *IEEE Transactions on vehicular technology,,* pp. 475-484., 2011.

[10] C. Attaianese, M. Di Monaco and G. & Tomasso, "Multi-source traction drive for axial flux permanent magnet in-wheel synchronous motor.," in *IEEE International Electric Machines & Drives Conference*, 2011.

[11] G. Rizzoni, L. Guzzella and B. M. Baumann, "Unified modeling of hybrid electric vehicle drivetrains," *IEEE/ASME transactions on mechatronics,* vol. 4, no. 3, 1999.

[12] D. Freudiger, M. D’Arpino and M. Canova, "A generalized equivalent circuit model for design exploration of li-ion battery packs using data analytics," *IFAC-PapersOnLine,* vol. 52, no. 5, pp. 568-573, 2019.

[13] M. D'Arpino, M. Cancian, A. Sergent, M. Canova and C. Perullo, "A simulation tool for battery life prediction of a Turbo-Hybrid-Electric Regional Jet for the NASA ULI Program," in *AIAA Propulsion and Energy 2019 Forum* , 2019.

[14] D. J. Wulpi, Failures of Shafts, vol. Volume 11: Failure Analysis and Prevention, ASM Handbook, 1986, pp. 459 - 482.

[15] Rexnord Industries, LLC, "Failure Analysis: Gears-Shafts-Bearings-Seals," 1978.

[16] A. H. Bonnett, "Cause, Analysis and Prevention of Motor Shaft Failures," *IEEE,* 1998.

[17] The International Organization for Standardization (ISO), "Rolling Bearings — Damage and Failures — Terms, Characteristics and Causes," 2017.

[18] R. L. Widner, Failures of Rolling-Element Bearings, vol. Volume 11: Failure Analysis and Prevention, ASM Handbook, 1986, pp. 490 - 513.

[19] L. E. Alban, "Systematic Analysis of Gear Failures," *American Society for Metals (ASM),* 1985.

[20] L. E. Alban, Failures of Gears, vol. Volume 11: Failure Analysis and Prevention, ASM Handbook, 1986, pp. 586 - 601.

[21] A. G. M. a. S. C. P. Lynwander, "Sprag Overriding Aircraft Clutch," 1972.

[22] J. G. Kish, "Advanced Overrunning Clutch Technology," AVRADCOM, 1977.

[23] Sikorsky Aircraft, "Helicopter Freewheel Unit Design Guide," AVRADCOM, 1977.

[24] AIA / AECMA, Project Report on Propulsion System Malfunction Plus Inappropriate Crew Response (PSM + ICR), vol. Volume 1, 1998.

[25] FAA Engine and Propeller Directorate, Turbofan Engine Malfunction Recognition and Response Final Report, 2009.

[26] C. Hendricks, N. Williard, S. Mathew and M. Pecht, "A failure modes, mechanisms, and effects analysis (FMMEA) of lithium-ion batteries," *Journal of Power Sources,* vol. 297, pp. 113-120, 2015.

[27] X. Shu, Y. Guo, W. Yang, K. Wei, Y. Zhu and H. Zou, "A Detailed Reliability Study of the Motor System in Pure Electric Vans by the Approach of Fault Tree Analysis," *IEEE Access,* vol. 8, pp. 5295-5307, 2020.